

<https://doi.org/10.15407/ujpe67.7.544>

N.V. BONDAR,¹ M.S. BRODYN,¹ YU.P. PIRYATYNSKYI,² N.A. MATVEEVSKAYA³

¹ Department of Nonlinear Optics, Institute of Physics, Nat. Acad. of Sci. of Ukraine
(46, Nauky Ave., Kyiv 03028, Ukraine)

² Department of Molecular Photoelectronics, Institute of Physics,
Nat. Acad. of Sci. of Ukraine
(46, Nauky Ave., Kyiv 03028, Ukraine)

³ Department of Crystalline Materials of Complex Compounds,
Institute of Single Crystals, Nat. Acad. of Sci. of Ukraine
(60, Nauky Ave., Kharkiv 61001, Ukraine)

STEADY-STATE SPECTROSCOPY AND SUB-NANOSECOND RESONANCE TRANSFER OF EXCITON EXCITATION ENERGY IN THE AQUEOUS SOLUTIONS AND FILMS OF ZnSe NANOCRYSTALS

Densely packed solid films of semiconductor nanocrystals (NCs) demonstrate specific optoelectronic properties owing to the strong quantum interaction between the NCs and the hybridization of exciton orbitals. This fact opens ways for creating new artificial light-harvesting complexes and photovoltaic structures with the spatial separation of electrons and holes. This work was aimed at the study of colloidal solutions and solid films of thioglycerol-stabilized ZnSe NCs by measuring their steady-state and time-resolved optical spectra. Relaxation and recombination of excitons via the surface and defect states of electrons and holes were found to prevail in NC solutions, whereas the quantum (internal) channel exciton relaxation dominates in NC films, which, according to the results of time-resolved measurements of photoluminescence spectra, is associated with the rapid (sub-nanosecond) transfer of exciton excitation energy in the films from smaller NCs to larger ones. Furthermore, intragap exciton states of two types were revealed in small ZnSe NCs after the oxidation and hydroxylation of their surface, as well as their unusual "dependence" on the NC size.

Keywords: exciton excitation energy, exciton, ZnSe, nanocrystal.

1. Introduction

The search for renewable energy sources is currently the most intensively studied area in condensed-state physics. One of such sources is the solar energy. Nowadays, devices based on crystalline semiconductors are used for its accumulation and conversion into electricity. In recent years, structures based on semiconductor nanocrystals (NCs) with the sizes of an order of the corresponding exciton Bohr radii and created in the form of superlattices or densely packed films attract the increasing attention because of their simple synthesis, wide absorption spectrum (AS), and narrow emission bands [1–8]. The functionalization of the NC surface with appropriate organic ligands allows

NCs to be used in biosensors and medical markers [3], light-emitting diodes (LEDs) and lasers, telecommunication networks and photovoltaic systems (3rd generation solar cells) [4–7].

Semiconductor NCs in combination with dyes, polymers, and J- or H-aggregates belong to the 2nd generation of photovoltaics. They act as artificial antennas like photosynthesizing structures, where chlorophyll molecules comprise a natural light-harvesting and transmitting antenna with a light energy conversion factor of about 0.97 [2]. However, the weak photostability together with narrow absorption and emission bands in those organic materials often restricts their applicability in nanohybrid systems [4, 5]. Recently, more and more preference has been given to NC-based nanostructures owing to their high stability with respect to long-term solar or laser radiation

and the possibility of an extensive restructuring of the adsorption and luminescence spectra as a result of the quantum size effect for excitons [5–8].

In spite of the progress achieved in the creation of NC films from the liquid phase, the rate and efficiency of the exciton excitation energy (EEE) transfer in them still remain low, which is associated with a number of problems [9–13]. Solid films in the form of NC superlattices or 2D layers form a material base, so the effective operation of devices on their basis is determined by the quantum interaction between the NCs. This interaction depends on the radius (the quantum size effect), the chemical structure, the length, and the number of ligands on the NC surface.

The quantum (electronic) interaction between the NCs, which arises owing to the presence of short ligands, is significantly affected by the dispersion of the NC sizes. As a result, the mechanism of transport of charge carriers has a hopping nature rather than a band-like one. In addition, owing to the quantum interaction, there appear new energy levels of electrons and holes, which substantially modify the optical properties of NC-based structures (this issue will be considered in the next paper).

The optical spectra of NC solutions and films are also affected by surface defects and broken bonds of external atoms, as well as by the energy and spatial (static) disordering [14–18]. Surface atoms comprise a considerable fraction of NCs (sometimes up to about 50%), and their defects and broken bonds form dense electron and hole states in the forbidden gap, which demonstrate a complicated dependence on both the NC size and the methods of solid film fabrication, such as spin-coating, drop-casting, or the Langmuir–Blodgett deposition technique [2, 4, 10, 13]. The amount of surface and deep NC defects in solutions and solid films can vary. Therefore, for a better understanding of the exciton relaxation mechanisms in the NC films, it is necessary to compare the corresponding optical spectra with their counterparts in the NC solutions. However, it should be noted that the vast majority of researches is devoted to studying NCs in either colloids or films separately. We are aware of only one work concerning PbS NCs [13], where the spectra of NC solutions and films were compared.

The unavoidable energy and spatial (static) disordering in NC films also affects the efficiency and

time of EEE transfer. The energy disordering induces a non-uniform broadening of the AS band owing to the dispersion of the energy levels of charge carriers that occupy the higher manifold of absorbing states in small NCs. After the excitation, they dissipate some of their energy before reaching the gap edge and transferring the energy to larger NCs [7, 10, 11]. Despite the fast relaxation (about 10 ps) toward the gap edge [1, 4], the competition between the processes of exciton capture by surface states, exciton cooling, and internal exciton recombination substantially prolongs the time of energy transfer and reduces the quantum yield of NC films.

On the other hand, the spatial (static) disordering in the films with the NC size dispersion is characterized by different coordination numbers (the number of contacts per one NC) for small and large NCs [12]. This disordering hampers the delocalization of the exciton wave function in the films and reduces the rate of excitation energy transfer [14–19].

Thus, a deep understanding of the mentioned difficulties should eliminate them, which would increase the rate and efficiency of EEE transfer, as well as the quantum yield, and give rise to the improvement of the optical and transport properties of NC-based structures.

In this paper, we present our results obtained while studying the colloidal solutions and densely packed films of small ZnSe NCs stabilized with the use of thioglycerol (TG) molecules. Time-resolved measurements of the photoluminescence (PL) intensity damping at room temperature testified to the ultrafast EEE transfer by short TG molecules, a considerable quantum-size dependence of the exciton energy, and the dense NC packing in the film. By combining the steady-state absorption and photoluminescence spectra, we discovered, for the first time, the in-gap (IG) states of charge carriers. These states lie by about 280 and 600 meV below the band gap edge in the NCs and are formed owing to the influence of water molecules on the NC surface. We found that, in the NC solutions, the intensity of IG and deep (defect) states is substantially higher than that of the quantum (internal) exciton states. However, in dense ZnSe NC films, due to the rapid and efficient EEE transfer, the quantum channel of exciton relaxation dominates, and the PL intensity of the IG and defect states decreases by almost an order of magnitude. The obtained data give us a broader understanding of the mechanisms of ex-

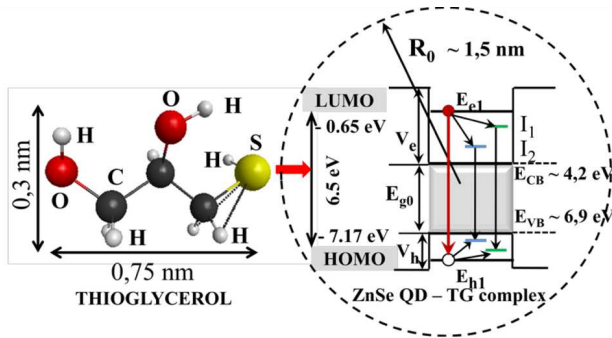


Fig. 1. (Left) The size and structure of the thioglycerol (TG) molecule. (Right) the energy diagram of the ZnSe NC + TG complex with the indicated energy transitions. E_{e1} is the 1S energy level of electrons, E_{h1} is the 1S energy level of holes, and $E_{g0} \approx 2.7$ eV is the forbidden gap width in crystalline ZnSe

citon relaxation in small ZnSe NCs and are favorable for the possible application of the latter in the 3rd generation solar cells and light-harvesting antennas.

2. Experimental Part

In this work, the colloidal solutions and solid films of small ZnSe NCs fabricated following the method described in our previous works [17, 18] are studied. Therefore, we will only briefly consider its main idea. According to our experimental result, we established that, in order to produce high-quality ZnSe NCs functionalized with TG molecules, the optimal molar ratio of components has to equal $[\text{Zn}^{2+}] : [\text{TG}] : [\text{Se}^{2-}] = 2 : 2.5 : 1$. An increase of the chalcogenide or TG fraction leads to an almost complete (5-fold) PL quenching of the specimens, but it can be restored by increasing the Zn fraction. Therefore, NCs with the Zn-enriched surface demonstrate PL induced by the quantum (core) exciton states, whereas the dominance of chalcogenides on the surface leads to the radiation emission mainly from the surface and deep states.

Taking the data of dynamic light scattering (DLS, Zetasizer Nano ZS) and the length of TG molecule (about 0.75 nm) into account, the average NC radius equals $R_0 \approx (1.5 \pm 0.1)$ nm (see Fig. 1). The R_0 -value was also calculated in the framework of the effective mass and “particle-in-spherical-box” models [2,3] for a finite-depth potential well and using the energy value for the main exciton transition in the AS. The average molar concentration of NCs in the solution was esti-

mated according to the Lambert–Beer law and taking the molar extinction coefficient of ZnSe NCs to equal $\varepsilon_{\text{mol}}(\lambda) = (8.6 \times 10^4 \div 2.4 \times 10^5) \text{ M}^{-1} \text{ cm}^{-1}$ for the NC radii $R = (1.4 \div 2.4)$ nm [20].

Solid films of ZnSe NCs were fabricated by drop-casting the colloidal solution onto a quartz substrate and additionally immersing the obtained specimens into the NC solution. After drying the specimens in the vacuum to remove excess moisture, dense and uniform NC films with a small number of cracks were obtained. The film thickness (of about 430 nm) was evaluated using a Tencor Alphastep 200 Profilometer (Tencor-Instruments).

The spectra of steady-state absorption and PL excitation (PLE) in the NC solutions and films were registered on UV spectrometers SHIMADZU UV-2450 (making use of a standard 10-mm quartz cuvette) and Perkin–Elmer Lambda LS-55 (Perkin–Elmer Instruments, UK) at room temperature. The PL quenching in the films was measured on a Life Spec-II spectrometer (Edinburgh Instruments Ltd.) with a resolution of about 4.0 ps using the time-correlated single-photon counting (TCSPC) method. A pulsed light-emitting diode with $\lambda_n = 255$ nm (≈ 40 W) and a picosecond laser EPL-405 with $\lambda_r = 405$ nm (≈ 5 mW) were used to register the steady-state and time-resolved PL spectra. After each measurement, the instrument response function (IRF) was also registered. Note that the intensity of laser pumping was low to avoid the generation of multiexciton absorption and Auger processes in separate NCs.

3. Discussion of the Results

3.1. Energy diagram of the complex ZnSe NC + TG

Before analyzing the optical spectra of the NC solutions and solid films, it is necessary to determine the type of the energy diagram for our ZnSe NC + TG complex, which, in turn, is determined by the relative arrangement of the energy levels of the electron and hole orbitals belonging to the NC and the ligand. This is the driving force for charge carriers and substantially affects the rate and efficiency of the EEE transfer.

If the energy diagram of the complex belongs to the first type (type-I), this means that the energy of the forbidden highest occupied molecular orbital–lowest unoccupied molecular orbital (HOMO–LUMO) gap

in the ligand completely overlaps its counterpart in the NC. As a result, excited excitons are localized in the NC, and the spatial separation of electrons and holes does not take place. If the complex belongs to the second type (type-II), then the HOMO-LUMO levels in the ligand and the NC are shifted by energy with respect to one another (the so-called band alignment), so the potential wells for electrons and holes are spatially located in different parts of the complex. In this case, the surface ligand, as a rule, is a hole acceptor that captures excited holes from the NCs, which results in a bathochromic (red) shift of the PL band [2].

To determine the energy diagram of our complex, we note that, when the NCs are synthesized, TG molecules become covalently bound to the NC surface as a ligand of the X-type owing to the affinity of the thiol group to Zn-chalcogenides, thus providing a chemical bond with Zn^{2+} at the NC surface [21]. As a result, the final position of the ligand's HOMO-LUMO levels with respect to their analogs in the ZnSe NCs determines the type of the energy diagram of our complex. According to the literature data [22], the energies of the conduction band minimum, E_{CB} , and the valence band maximum, E_{VB} , in crystalline ZnSe lie by about 4.2 and 6.9 eV, respectively, below the vacuum level (see Fig. 1).

When calculating the HOMO-LUMO levels and the TG bandgap energy, the method of density functional theory and the B3LYP DFT-D4, 6-31++G(3d,3p,f) software package were used. As a result, the values for the HOMO (-7.17 eV), the LUMO (-0.65 eV), and the TG band gap (≈ 6.5 eV) were calculated. By comparing the corresponding energy levels in the NC and TG, one can see that the complex ZnSe NC + TG is a heterostructure of the first type, because the forbidden gap in ZnSe (≈ 2.7 eV) is completely overlapped by the TG band gap. This fact means that the potential wells in which the excited electrons and holes are localized are located in the ZnSe NCs (see Fig. 1).

The energy diagram of our complex differs substantially from, for example, those for similar complexes CdSe NCs + thiols and CdS NCs + phenyldithiocarbamate [2, 21]. The indicated complexes belong to the structures of the second type, because their ligands are hole acceptors that capture excited holes from the NCs, which leads to the bathochromic shift and the rapid PL quenching. The calculated values of the en-

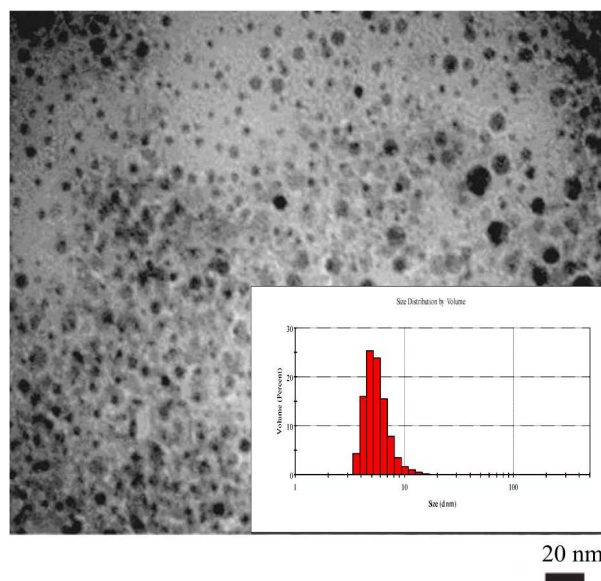


Fig. 2. TEM image and (the inset) the histogram of the size distribution of ZnSe NCs according to DLS data

ergy levels in the NC and TG also make it possible to estimate the depths of potential wells for electrons and holes in the NC (see Fig. 1): $V_e \approx -3.55$ eV and $V_h \approx -0.276$ eV. As a result, we can calculate R_0 more accurately (see below), whereas the application of the model of “infinitely deep potential well” introduces an error of about 11%.

3.2. Steady-state absorption and photoluminescence spectra of aqueous ZnSe NC solutions

In order to understand the processes of exciton relaxation and radiation emission in such a complex system with the interaction between NCs as a densely packed film, let us firstly analyze those processes in a simpler system, namely, separate NCs in the solution. The vast majority of NCs in the solution are separate, but a small number of them can be found in the form of aggregates, as one can see in Fig. 2. This is a certain drawback of our synthesis method, but the aggregates do not significantly affect the overall spectrum emitted by the NC solution. Figure 3 illustrates the normalized AS of the aqueous solution of ZnSe NCs (the black curve). One can see that its contour contains several peaks. Owing to the quantum-size effect, the peaks are shifted to the blue (short-wavelength) side of the spectrum with respect to the

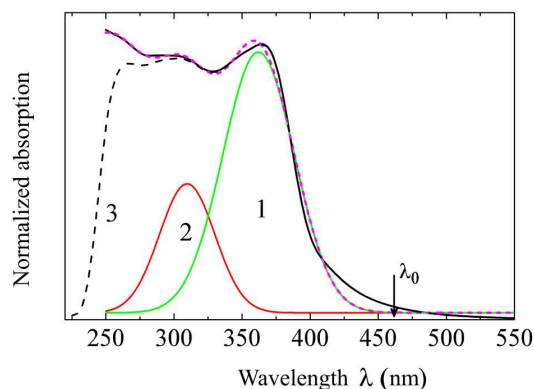


Fig. 3. Normalized AS of the aqueous solution of ZnSe NCs (black curve) and its resolution into Gaussian functions 1 (green curve) and 2 (red curve); the dashed purple curve is their sum; curve 3 (dashed black curve) is the result of the subtraction of the AS for pure TG from the AS for the NC solution. $\lambda_0 \approx 461$ nm is the position of the band gap edge in crystalline ZnSe

ZnSe band gap: $\lambda_0 \approx 461$ nm (marked by the vertical arrow).

In order to determine the positions of AS peaks and the energies of allowed one-photon exciton transitions in the NCs more accurately, the AS contour was fitted (using the OriginPro mathematical package) with Gaussian functions. As a result, two curves with maxima at about 362 nm (curve 1) and about 310 nm (curve 2) were obtained. To avoid uncertainties within the wavelength interval of those curves, we also registered the AS of pure TG in the aqueous solution with the same molar concentration as was in the ZnSe NC solution, which did not demonstrate any characteristic features in this interval [17,18]. The AS of ZnSe NCs without the influence of surface ligands was calculated by subtracting the AS of pure TG from the original AS of ZnSe NCs. The resulting curve 3 in Fig. 3 has peaks the positions of which clearly coincide with those in the initial AS. From Fig. 3, one can also see that the absorption in the ZnSe NC solution at higher energies ($\lambda \leq 250$ nm) occurs due to the organic and aqueous media, where the NCs were synthesized.

Next, according to our calculations, the first and second AS bands are created by the transitions of excitons in the ground ($1S_e - 1S_{3/2(h)}$) and excited ($1S_e - 2S_{3/2(h)}$) NC states. The full width at half maximum (fwhm) of the first AS band is a result of the size dispersion of NCs and equals about 300 meV,

and the blue shift of this band occurring due to the quantum-size effect equals about 650 meV. Using the effective mass model (“particle-in-spherical-box”) [2,3], as well as the values of the $1S$ transition energy (about 3.42 eV) and $V_{e(h)}$, we calculated the value $R_0 \approx (1.5 \pm 0.1)$ nm, which is in good agreement with our DLS data.

To induce PL in the solutions, we excited them with a laser with $\lambda_n = 255$ nm (≈ 4.86 eV) and a photon energy lower than the TG bandgap width, which allowed us to perform sub-barrier (resonance) excitation of ZnSe NCs. The resulting PL band is shown in Fig. 4 (the solid black curve). It is worth noting that the obtained band is rather broad and typical of Zn and Cd chalcogenide NCs with small radii of 1–2 nm [5, 11, 23], because it is a result of the band overlapping of excitons from the quantum (core) NC states, as well as transitions of electrons and holes localized at the surface and deep defects. The reduction of the NC radius induces the growth of the PL band width owing to the increase of the amount of NC surface atoms (as compared to the internal ones) and their dominating contribution to radiation emission [11]. On the contrary, for the NC radii larger than 2 nm, the band becomes narrower due to the dominant contribution of exciton states, the intensity of which increases exponentially in comparison with the surface states (see [11, Fig. 4]). Thus, the selected sizes (about 1.5 nm) of ZnSe NCs are optimal for the simultaneous study of excitons in the internal and surface NC states, as well as their interaction.

Several peaks are discernible on the PL band contour. Their exact positions were also determined by fitting the contour with Gaussian functions. It was found that the contour shape can be optimally fitted using five Gaussians. The latter were divided into three groups. The first group includes the Q band with a maximum at about 366 nm and fwhm ≈ 294 meV, which is formed by exciton emission from the quantum NC states. This is evidenced by the position of its peak, which practically coincides with the position of the $1S$ transition peak in the AS (shown by the thick vertical arrow). A small discrepancy of about 4 nm between the peak positions is a result of the electrostatic compression of the exciton wave function owing to the interaction of the thiol group with the surface Zn atoms [17, 18]. One can see that the Q band is relatively narrow, and its fwhm value is in good agreement with the corresponding value for

band 1 in the AS, thus testifying that the absorption and emission in this spectral interval are governed by the internal exciton states. The obtained data have to be supplemented with the PL excitation (PLE) spectrum. Unfortunately, the latter was not registered. However, the research of similar solutions of CdSe and CdS NCs showed that the position of the PLE spectrum coincides well with the AS and steady-state PL positions in the solutions, where there is no interaction between NCs [7, 16, 23].

The most interesting is the second group of bands in Fig. 4, which lie in the forbidden NC gap and are denoted as IG states. In comparison with the well-studied quantum states of excitons, the nature and the sources of IG states are currently the most debated issues [9–11]. So far, it has been established that in Zn and Cd chalcogenide NCs, IG states form nonpassivated surface atoms Se, S, or Te, whose localized levels lie about 500 meV above the valence band maximum [11]. Electrons do not form such states, since their mass is small as compared to that of holes, and because ligands mainly passivate the surface atoms of metals.

The study of IG states is an important problem, because, together with the internal states, they form the total PL band and determine its quantum yield. Because of their low dipole moment and oscillator strength, they have a low absorption intensity and, in our case, manifest themselves only as the long-wavelength broadening of the AS tail in the wavelength interval above 410 nm, as can be seen from Fig. 3. To our knowledge, these states were first discovered in ZnSe NCs, although similar states were registered in solutions of CdSe NCs with radii less than 2 nm [10].

Although the source of formation of IG states has not been established exactly, it is supposed that it may be related to the influence of aqueous solution on the surface of ZnSe NCs. The results of theoretical calculations in works [5–8] testify that if the synthesis is performed in aqueous solutions, there appear two types of states in the band gap of ZnSe NCs. Their common feature is the independence of their energy positions of the radii of synthesized NCs. On the basis of calculations made by the cited authors, we came to the conclusion that the band I_1 with the peak at about 394 nm and lying by about 280 meV below the gap edge can be formed owing to the oxidation of surface Zn atoms, because the synthesis of our ZnSe

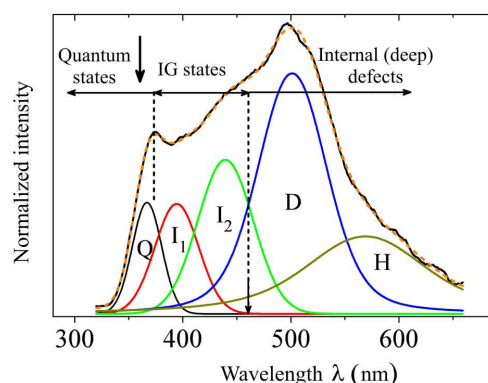


Fig. 4. PL spectrum (solid black curve) of aqueous ZnSe NC solutions under the laser excitation with $\lambda_n = 255$ nm and its resolution into Gaussian profiles: Q (black), I_1 (red), I_2 (green), D (blue), and H (black-yellow). The dashed orange curve is their sum. The thick vertical arrow marks the position of the $1S$ transition in the AS, and the thin vertical one corresponds to λ_0

NCs did not involve the application of inert atmosphere (argon or nitrogen). As one can see below, the position of this band does not depend on the NC radius, and its substantial intensity is associated with the fact that it resonates with the $1S$ states of NCs of a definite size. According to our calculations, this occurs in NCs with $R \approx 1.9$ nm. In larger NCs, the red shift of the Q band makes the energy position of the I_1 band higher, and, therefore, the I_1 band does not appear in the PL spectrum (see Section 3.3). The other band I_2 (at about 440 nm), which lies by about 600 meV below the gap edge, resonates only with $1S$ states in NCs with $R \approx 3.4$ nm. This value exceeds the largest size of separate NCs in our solutions or films by almost 1 nm; therefore, the resonance conditions for this band are realized not in separate NCs, but in their aggregates.

Finally, the third group consists of bands D (at about 500 nm) and H (at about 560 nm), which lie well below not only the band gap edge in NCs, but also λ_0 . Those bands are often observed in undoped crystalline ZnSe and originate from electron transitions onto deep defect hole states (deep hole levels). Therefore, since the corresponding wave functions are strongly localized, they do not perceive the NC boundaries. The normalized integral areas of the bands equal 1 for Q , 1.5 for I_1 , 4.2 for I_2 , 9.5 for D , and 3.6 for H . The indicated values testify that the dominant recombination channels in ZnSe NC solu-

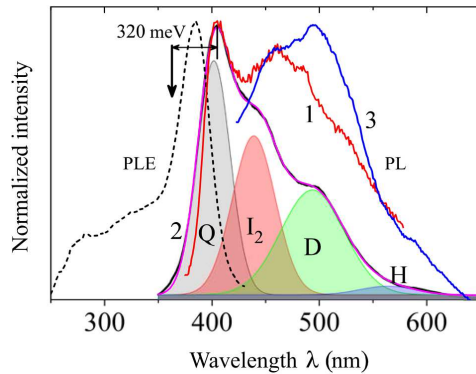


Fig. 5. Steady-state PLE and PL spectra of solid ZnSe NC films: lamp excitation at $\lambda = 300$ nm (1, red curve), excitation at $\lambda_n = 255$ nm (2, black curve), excitation at $\lambda_r = 405$ nm (3, blue curve). The vertical arrow marks the position of the 1S peak in the AS of the NC solution. Bands Q, I_2 , D, and H were obtained by fitting the curve shape with two Gaussian functions, and the dashed purple curve is their sum

tions are IG states and deep states of charge carriers. This is a result of the quality of synthesized NCs, as well as the film excitation with λ_n . The excitation generates “hot” electrons and holes. At the beginning of the cooling process, those electrons and holes become rapidly (10–20 ps) captured by the IG and defect states in the NCs, thus reducing the population of quantum states. As will be shown below, the situation is radically different in solid films with the interaction between NCs, where the EEE transfer process plays a significant role.

3.3. Steady-state photoluminescence spectra of solid ZnSe NC films

In this subsection, we analyze the optical spectra of solid ZnSe NC films and show that their drastic differences from the spectra of NC solutions are a result of the quantum interaction between NCs and the EEE transfer in the film plane.

The hybridization of exciton orbitals, which takes place owing to the interaction between NCs in the films, leads to the spectral reconstruction of their energy levels, which affects the spectral position of the emission and absorption bands. Unlike the colloidal NC solutions, where the corresponding peaks in the PLE, PL, and absorption spectra practically coincide with one another, in the case of NC films, they are shifted not only to the red side of the spectrum, but also with respect to one another. The origins of the

shift are different for different spectra, and they will be discussed in more details in the next paper. Here, we will briefly dwell on the main points.

The application of the PLE method in order to determine the energies of excited states by detecting the intensity of radiation emission from 1S or surface states is quite widespread [5, 6, 15]. When registering the corresponding PLE spectrum, the detection wavelength (in our case, at the surface state position, $\lambda_{\text{det}} = 460$ nm) and the excitation flux intensity are maintained fixed, but the energy of an excitation photon is varied. The resulting PLE band is shown in Fig. 5. If the relaxation processes are fast enough, the PLE band demonstrates states with enhanced absorption, but its spectral position does not always coincide with the 1S peak in the AS of the films. It is worth noting that this peak was also registered. However, since it turned out rather unstructured and blurred, we do not present it here.

From Fig. 5, one can see that the peak of the PLE band is red-shifted by about 180 meV with respect to the energy of the exciton 1S transition in the solution AS (shown by the thick vertical arrow). The shift takes place owing to the quantum interaction between the NCs. As a result, the hybridization of charge carrier orbitals [8] leads to the formation of a new set of quantum exciton levels in the NC film.

Besides the PLE band, Fig. 5 also demonstrates three PL bands excited with the use of different excitation sources: curve 1 corresponds to the lamp excitation with $\lambda = 300$ nm (Perkin–Elmer Lambda LS-55), curve 2 to the laser excitation with $\lambda_n = 255$ nm, and curve 3 to the laser excitation with $\lambda_r = 405$ nm. We present the PL bands registered for different excitation sources in order to illustrate the differences in their shapes. In some works [16, 23], the PL band for NC films was obtained only for the lamp excitation of specimens. As a result, the information about the surface and deep exciton states was lost. By comparing the positions and shapes of the PL bands for the NC solution (Fig. 4) and the NC film (Fig. 5), one can observe substantial differences between them. The main difference is the red (long-wave) shifts of the PL band by about 320 meV with respect to the 1S transition in the solution AS and by about 140 meV with respect to the PLE peak. Unlike the latter, the shift of the PL band is induced by the migration of excitons in the film from smaller NCs to larger ones (see below). The reorganization of the

energy levels of excitons, as well as the mechanisms and modes of the EEE transfer, will be discussed in the next paper in more details.

Now, let us consider a relation between the shift magnitude of the steady-state PL band and the size of ZnSe NCs in the film, and analyze its shape peculiarities appearing at various excitation methods. In Fig. 5, PL band 1 (the red curve) was registered under the lamp (weak) excitation. It consists of two subbands: a narrower short-wavelength subband with its peak at about 404 nm and a broad long-wavelength one with its peak at about 460 nm. The mixing of such dual emission provides the light gray color of our NC films. It is worth noting that such a general shape of the PL band at a weak excitation is typical of small NCs. It is also observed in films with CdSe or CdS NCs 1–2 nm in radius [9, 11, 23].

First of all, let us determine which NC size corresponds to the peak of the PL band at about 404 nm. Using the “particle-in-spherical-box” model [2, 3], we calculated that these are NCs with $R_c \approx (2.2 \pm 0.1)$ nm. Hence, the above-mentioned red shift of the short-wavelength PL band is indeed caused by the migration of excitons from smaller ZnSe NCs (with a higher energy of the forbidden gap) to larger ones via incoherent exciton jumps between them. In the course of exciton migration, the exciton energy and velocity decrease owing to the mitigation of the quantum-size effect and the overlapping of the wave functions whose amplitudes decay exponentially outside the NCs [2, 3]. As a result, excitons become able to reach NCs with the size R_c , where the probability of their further migration drops sharply.

The described process of exciton migration in the film is important not only from the physical viewpoint, but also from the application one. For example, a ZnSe NC film can be coated onto the surface of another semiconductor, so a spatial separation of electrons and holes may arise at the interface, which is a basis of the operation of light-harvesting antenna systems and photovoltaic structures [1–3]. The obtained result makes it possible to classify all NCs into NC donors (with $R < R_c$) and NC acceptors (with $R \geq R_c$), and determine the ratio $R_0/R_c \approx 0.7$. This parameter characterizes the NC film as an artificial antenna: the smaller the ratio is, the longer the exciton migration path is, and the larger number of NCs is involved in the process of EEE accumulation and transfer.

Note that, besides the quantum energy of excitons, the width of the tunnel barrier between the NCs (the length of the ligand molecule) and its height (the value of the HOMO–LUMO gap in the ligand) also affect the value of the ratio R_0/R_c : the larger they are, the shorter the migration length of excitons in the film is, and the lower its efficiency as an artificial antenna is. While synthesizing NCs, long ligands are often used, e.g., trioctylphosphine oxide (TOPO) or oleic acid, with a molecular length of more than 1.5 nm. They either strongly weaken the exciton migration and the EEE transfer or completely suppress them. Therefore, long ligand molecules are tried to be replaced with shorter ones [1–3, 5, 13].

The width of the long-wave PL band located at about 460 nm testifies that this band can be formed owing to the overlapping of several bands, which cannot manifest themselves separately under a weak lamp excitation. In order to prove this statement, we recorded the PL band, when the film was laser-excited with the wavelength λ_n (Fig. 5, the black curve). Note firstly that the short-wave bands are formed by excitons in the quantum NC states, and their positions under both excitation methods coincide well with each other, but the long-wave sections of those bands are different.

As one can see from Fig. 5, if the film is excited at λ_n , the long-wave section of the PL spectrum demonstrates a structure consisting of several overlapping bands. To determine their positions, the general contour of PL band 2 was fitted with Gaussian distributions. As a result, we obtained some simpler bands: Q (≈ 402 nm), I_2 (≈ 440 nm), D (≈ 497 nm), and H (≈ 565 nm). The last three bands coincide well with their analogs in the NC solution. At the same time, the I_1 band does not appear in the steady-state PL spectrum. This is a result of the red shift of the Q band, which made the position of the I_1 band higher by energy. Therefore, the latter does not appear in the PL spectrum, or it has disappeared because of a possible improvement of the surface stoichiometry in larger NCs.

For verification, we estimated the fwhm parameter for the Q band and obtained a value of about 291 meV, which coincides with its counterpart for the colloidal NC solution. However, this value has to be smaller (about 170 meV), because small ZnSe NCs do not contribute to the fwhm magnitude. Thus, the only reason for the broadening of the Q band is

the I_1 one, which does not disappear, when the NC size increases. This can be seen, if we compare the short-wave sections of the Q band under the lamp and laser excitations (Fig. 5). When becoming higher in energy, the I_1 band enters the interval of excited states in large NCs and can participate in the EEE transfer [25].

Furthermore, after comparing the normalized integral areas of the obtained bands: Q (1), I_2 (0.89), D (0.87), and H (0.06) with the corresponding results for the colloidal NC solution, one can see that they became several times smaller. This could be a consequence of improvements in the crystalline structure of NCs during the film formation, as well as the reduction of their internal defects. However, the temperature of the specimen synthesis was too low (lower than 100 °C) to affect the NC surface and the ZnSe crystal lattice during the aqueous solution evaporation. The reason for this consists in the rapid (subnanosecond) EEE transfer to emitting NCs. In other words, since the “horizontal” EEE transfer in the films to emitting NCs is faster than the “vertical” energy relaxation of electrons and holes in separate NCs, the quantum channel of exciton relaxation and emission in dense films becomes dominating. This is also one of the main features that distinguishes the exciton relaxation processes in solutions and films, with the strong interaction between NCs in the latter.

The independence of the I_1 and I_2 bands of the NC radius was also observed in the nanostructures of other semiconductors. The authors of work [24] revealed a similar behavior of IG bands in small CdSe NCs and showed that it is an attribute of electron and hole states with the so-called pinning nature. In other words, those electron and hole states have a fixed energy and can be located either higher by energy than the $1S$ transition in NCs with radii larger than 2 nm or lower, i.e., inside the forbidden gap in NCs with radii smaller than 1.5 nm. Such behavior takes place because of the substantial localization of the wave functions of IG states, which do not feel the NC boundaries. For example, the red shift of the Q band in our NCs with $R_c \approx 2.2$ nm makes it lower in energy than the I_1 band, but it remains higher in energy than the I_2 band. If the NC radius increases further, the bands I_1 and I_2 become higher than the Q one, enter the interval of excited NC states, and participate in the EEE transfer [25]. Such behavior of the bands I_1 and I_2 confirms the sources of their

origin [5,6], as well as the existence of pinned exciton states in ZnSe NCs [24].

As was mentioned above, the excitation of our NC films at λ_n creates “hot” electrons and holes, which quickly relax and mainly populate the IG and deep (defect) states thus determining the profile of the PL band in the solution. To avoid those processes, it is necessary to substantially reduce the energy of NC excitation. For this purpose, we used a laser with $\lambda_r = 405$ nm (≈ 3.06 eV, ≈ 5 mW). The obtained PL band \mathcal{P} is shown in Fig. 5 (the blue curve). The variation of the pump intensity from 0.5 to 5 mW did not reveal appreciable changes in the shape of the PL band \mathcal{P} and the positions of its peaks (not shown in the figure), which coincides well with similar results obtained at λ_n .

With the increase of the laser pump intensity, the emission growth rate remained the same for all peaks in the band. This fact testifies to the weak interaction between the IG and deep (defect) states of electrons and holes. However, we do not manage now to explain the nonlinear growth of the integral areas of those bands with the laser pump intensity. The absence of a spectral shift of the I_2 band at various laser pump intensity levels is another confirmation that the IG states are created by sole localized levels of electrons and holes rather than their discrete set at the NC surface.

To summarize, we note that similar IG bands of PL were also observed in CdSe NCs stabilized by octadecylamine [10], but the cited authors did not determine the source of the band origin. Therefore, after having compared the steady-state optical spectra of the ZnSe NC solutions and films, we revealed, for the first time, the IG states of excitons in the forbidden gap of NCs and their unusual “dependence” on the NC size.

3.4. Sub-nanosecond EEE transfer and dynamics of exciton decay in dense ZnSe NC films

The results of steady-state spectroscopy of solid NC films testify to the presence of the EEE transfer process as a result of the quantum interaction (orbital hybridization) between the NCs. But they cannot be regarded as a direct evidence for this process. To obtain the direct evidence, time measurements of the PL intensity damping, as well as the determination of the shape of the PL bands emitted by NC films, are required.

Figure 6 demonstrates the normalized kinetic curves of PL quenching at wavelengths of 370, 380, 390, and 405 nm measured on the short-wave wing of PL band 2 (Fig. 5) under the excitation at $\lambda_n = 255$ nm (about 4.86 eV). From the figure, one can see that the quenching time increases (the quenching rate decreases) as the registration wavelength – or, accordingly, the NC radius – grows.

While obtaining an analytic expression for the quenching curve, one should bear in mind that, in the simplest case where the damping in a system is characterized by a single rate parameter, the shape of the corresponding curve is also described by a single exponential function [2, 3]. If the damping has a more complicated behavior characterized by some rate distribution, the fitting of the curves is much more difficult.

The experimental PL quenching curves depicted in Fig. 6 can be fitted well using the bi-exponential function

$$I(t) = A_1 \exp\left(-\frac{t}{\tau_1}\right) + A_2 \exp\left(-\frac{t}{\tau_2}\right),$$

where $A_1(A_2)$ and $\tau_1(\tau_2)$ are the amplitude and quenching time, respectively, of the fast (slow) component [17]. An example of the fitting for the curve corresponding to $\lambda = 370$ nm is shown by the dashed black curve. The λ -dependences of the fitting parameters τ_1 and τ_2 within the interval of $\lambda = (370 \div 420)$ nm with the increment of 5 nm are shown in Fig. 7. The corresponding limits for the fitting parameter R (the NC radius) are also indicated in the figure.

A similar bi-exponential dependence of the PL quenching is often observed in NC films of II-VI semiconductors, for example, CdSe and CdS [2, 9–11]. One should also bear in mind that the function $I(t)$ can be more complicated, e.g., three-exponential or Kohlrausch, if, besides the EEE transfer and internal recombination, the processes of charge carrier capture onto surface states and deep traps also play a significant role in the PL band quenching [2, 3].

As one can see from Fig. 7, the values of the parameters τ_1 and τ_2 are different by almost an order of magnitude. This is so, because they describe different physical processes, where excitons are engaged. The fast component is responsible for the time of exciton resonance tunneling from small to large NCs (the EEE transfer time), whereas the slow component is the sum of the radiative and non-radiative lifetimes

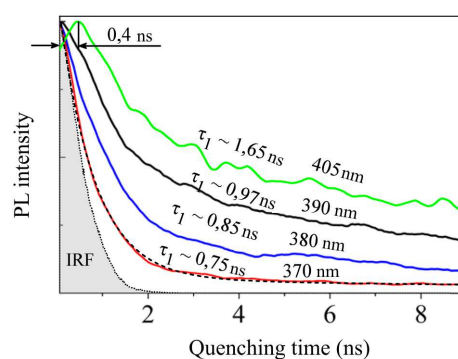


Fig. 6. Curves of PL intensity quenching at some wavelengths and the corresponding τ_1 -values. The black dashed curve is the approximation of the curve for $\lambda = 370$ nm by the function $I(t)$. IRF is the instrument response function

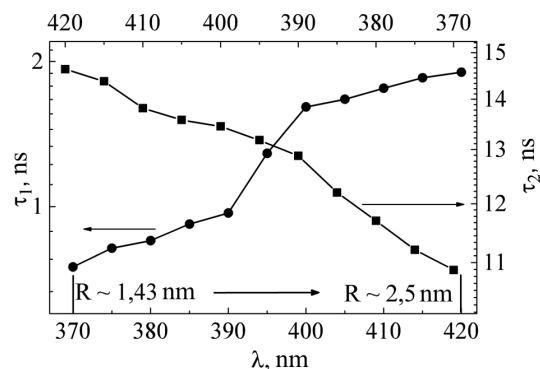


Fig. 7. λ -dependences of the fitting parameters τ_1 and τ_2 for the PL quenching curves within the interval $\lambda = (370 \div 420)$ nm. The limits for the fitting parameter R (the NC radius) are also indicated

in the NCs, $\tau_2 = \tau_r + \tau_{nr}$. The value of τ_1 rapidly increases within the interval near $\lambda \approx 400$ nm. Then, its growth rate slows down because of a significant weakening of the EEE transfer in NCs with $R \geq R_c$, whereas τ_2 smoothly increases as a result of the exciton lifetime growth in NCs.

These results can be used to estimate the exciton diffusion length L in the NC film. Before reaching NCs with $R \geq R_c$, where the exciton radiative damping takes place, excitons make $n = \tau_2/\tau_1$ jumps from one NC to another one. Therefore, putting $\tau_1 \approx 1$ ns and $\tau_2 \approx 13$ ns (Fig. 7), we obtain $L \approx n(2R_0 + \lambda) \approx 50$ nm. Next, from Fig. 6, one can also see that the PL quenching for wavelengths $\lambda \leq 400$ nm begins immediately after the excitation pulse termination. At the same time, for $\lambda > 400$ nm, the PL intensity continues to grow for some time. This was shown using

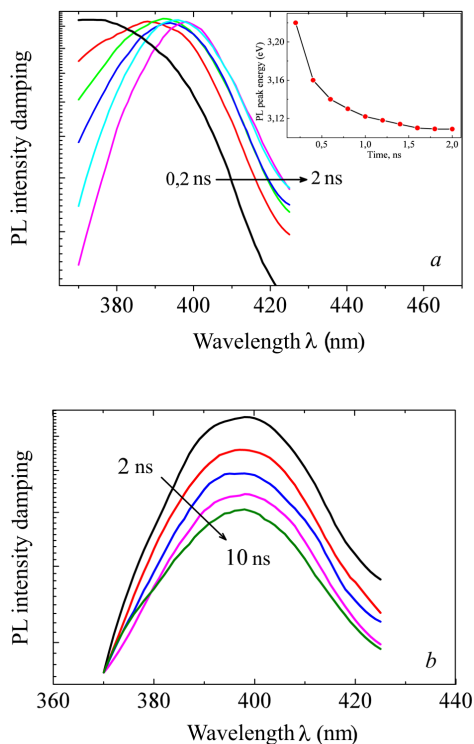


Fig. 8. Quenching dynamics of the PL band at about 404 nm in various time intervals: 0.2–2 ns (a) and 2–10 ns (b). The inset in panel a illustrates the red shift of the band maximum

the curve for $\lambda = 405$ nm as an example. One can see that the PL intensity increases further during about 400 ps and begins to decrease afterward. The same situation is observed for other quenching curves corresponding to $\lambda > 405$ nm [17].

In order to understand the process of PL intensity damping in dense NC films, it has to be compared with a similar process in molecular donor-acceptor systems [2, 3]. In the latter, the rate of PL intensity damping is known to be driven by the mechanism of weak dipole-dipole interaction. It is described by the Förster resonance energy transfer and is proportional to $\tau_D(R_0/r)^{-6}$, where τ_D is the donor damping in the absence of an acceptor, R_0 the Förster radius, and r the distance between the nearest donor and acceptor [3, 26]. Besides the distance, the interaction in donor-acceptor systems is also determined by the overlap integral of the donor emission and acceptor absorption spectra.

The rate of PL quenching can increase with the acceptor concentration growth in the system, pro-

vided that every donor is surrounded by several acceptors [3]. In solid films with a random dense or loose packing of NCs, the distance between the surfaces of neighbor NCs remains almost constant and proportional to the length of the ligand molecule (in our case, it is about 0.75 nm). Then, why does the time of PL quenching increase (the rate of PL quenching decreases) as the radiation wavelength grows (as is shown in Fig. 6)?

For explanation, instead of the distance between the NCs, we have to consider their coordination number or the average number of contacts per NC in the film. If a solid film consists of NCs possessing the same size, the coordination number varies from about 4.4 for the random loose packing to about 5.9 for the random close packing [12]. If the sizes of NCs have the Gaussian or normal logarithm distribution, then the coordination number of large NCs is about 3 to 4 times larger than that of small ones [12]. As a consequence, the coordination number of a selected NC will consist of NCs with various sizes and, therefore, with various exciton energies, which will hinder the EEE transfer and reduce its rate.

In particular, for small ZnSe NCs (at the beginning of the distribution function) emitting at about 370 nm, the PL quenching rate is the highest despite their lowest coordination number. The reason is as follows. Although they have a small coordination number, they possess a large quantized exciton energy and are in contact with the dense manifold of higher-lying excited states in large NCs, which is an analog of the overlap integral in donor-acceptor systems. As the NC radius and coordination number increase, the overlap integral and the EEE transfer rate decrease. On the contrary, the internal PL increases owing to the exciton recombination, which can be observed in Figs. 5 and 6 for $\lambda \geq 380$ nm.

On the other hand, for large NC acceptors with $R \geq R_c$ (in the distribution function tail), the coordination number is the largest, and it mainly consists of small NC donors that block the EEE transfer. This is another reason responsible for the peak position in the steady-state PL band at about 404 nm.

On the basis of this picture, we can explain the growth of the PL intensity during about 400 ps after the termination of the excitation pulse. It is induced by the sum of the own PL of NC acceptors and the exciton flow from the NC donors located on their surface (see Fig. 6).

Note that the growth of the PL intensity is observed for all wavelengths within the interval of 405–420 nm [17]. The value of τ_1 in this interval determines not the time of EEE transfer between the NCs, but the time of charge carrier capture onto the surface and deep states of NCs.

We supplemented the presented material with the results of measurements concerning the quenching dynamics of the PL band shape within various time intervals. Figure 8 demonstrates the shape damping of the PL band at about 404 nm (Fig. 5) within a spectral interval of 370–425 nm in various time intervals: 0.2–2 ns (panel *a*) and 2–10 ns (panel *b*) after the excitation pulse termination.

From Fig. 8, *a*, one can see that, at about 200 ps after the excitation pulse, the PL band is broad (the black curve), being formed by the majority of excited NCs. As time goes by, small NCs quickly transfer the excitation energy to larger ones, so the intensity of the short-wave band wing decreases, and the band becomes red-shifted (see the inset in Fig. 8, *a*). At about 2 ns after the termination of the kinetic processes with the participation of excitons that reach NC acceptors, the value of τ_1 becomes almost stable (Fig. 7), and the shape and peak of the PL band practically coincide with their analogs at the steady-state excitation. As time goes further from 2 to 10 ns, the shape and spectral position of the PL band do not change. Only a decrease in the band intensity is observed (Fig. 8, *b*), which is a result of the exciton recombination and capture onto the surface and non-radiative states. Thus, using the results obtained for the kinetics and dynamics of the intensity and shape damping of the PL band, we have indisputably evidenced the presence of the EEZ transfer in dense ZnSe NC films.

4. Conclusions

In this work, the results of optical and spectroscopic studies of ZnSe NC colloids and solid films obtained on the basis of combined steady-state and time-resolved measurements have been compared. We confirmed that the main channels of the exciton recombination in separate NCs in the solutions are the surface and deep defect states of electrons and holes. However, in solid NC films, owing to the rapid EEE transfer, the recombination through quantum (internal) exciton states prevails, which reduces the relaxation path of “hot” excitons to the exciton states in

the NCs due to the quantum interaction between the latter. By combining the kinetic and dynamic measurements of the PL band intensity damping, we revealed an ultrafast (sub-nanosecond) EEE transfer in the array of ZnSe NCs associated with the high exciton energy (the small size of ZnSe NCs) and the short length of TG molecules.

By summarizing our data and those of other authors, we have shown, for the first time, that there are two types of IG states in small ZnSe NCs, which are caused by the influence of the aqueous medium on the surface of NCs. We have found that the positions of those states do not depend on the NC size, so those states can participate in the EEE transfer and increase the efficiency of this process.

The obtained results provide a clear understanding of the evolution of the exciton relaxation and emission processes when switching from ZnSe NC colloids to solid ZnSe NC films. This can bring us closer to the creation of artificial photovoltaic structures and light-harvesting complexes possessing the characteristic features of natural photosynthetic mechanisms.

1. M. Achermann, M.A. Petruska, D.D. Koleske, M.H. Crawford, V. I. Klimov. Nanocrystal-based light-emitting diodes utilizing high-efficiency nonradiative energy transfer for color conversion. *Nano Lett.* **6**, 1396 (2006).
2. R.D. Harris, S.B. Homan *et al.* Electronic processes within quantum dot-molecule complexes. *Chem. Rev.* **116**, 12865 (2016).
3. N. Hildebrandt, Ch.M. Spillmann, W.R. Algar *et al.* Energy transfer with semiconductor quantum dot bioconjugates: A versatile platform for biosensing, energy harvesting, and other developing applications. *Chem. Rev.* **117**, 536 (2017).
4. P. Nagpal, V.I. Klimov. Role of mid-gap states in charge transport and photoconductivity in semiconductor nanocrystals films. *Nat. Comm.* **2**, 486 (2011).
5. J. Min, Ying Zhang, Y. Zhou, D. Xu, Ch. S. Garoufalis, Z. Zeng, H. Shen, S. Baskoutas, Yu Jia, Z. Du. Size engineering of trap effects in oxidized and hydroxylated ZnSe quantum dots. *Nano Lett.* **22**, 3604 (2022).
6. V.V. Nikesh, A.D. Lad, S. Kimura, Sh. Nozaki. Electron energy levels in ZnSe quantum dots. *J. Appl. Phys.* **100**, 113520 (2006).
7. Min Gao, H. Yang, H. Shen, Zaiping Zeng, Fengjia Fan, Beibei Tang, Jingjing Min, Ying Zhang, Qingzhao Hua, Lin Song Li, Botao Ji, Zuliang Du. Bulk-like ZnSe quantum dots enabling efficient ultranarrow blue light-emitting diodes. *Nano Lett.* **21**, 7252 (2021).
8. W. Jaskolski, G.W. Brayany *et al.* Artificial molecules. *Int. J. Quant. Chem.* **90**, 1075 (2002).

9. D. Jasrasaria, J.P. Philbin, Ch. Yan, D. Weinberg, A.P. Alivisatos, E. Rabani. Sub-bandgap photoinduced transient absorption features in CdSe nanostructures: The role of trapped holes. *J. Phys. Chem. C* **124**, 17372 (2020).
10. B.R. Watson, W.B. Doughty, T.R. Calhoun. Energetics at the surface: Direct optical mapping of core and surface electronic structure in CdSe quantum dots using broadband electronic sum frequency generation microscopy. *Nano Lett.* **19**, 6157 (2019).
11. A. Veamatahau, B. Jiang, T. Seifert, S. Makuta, K. Latham, M. Kanehara, T. Teranishi, Y. Tachibana. Origin of surface trap states in CdS quantum dots: Relationship between size dependent photoluminescence and sulfur vacancy trap states. *Phys. Chem. Chem. Phys.* **17**, 2850 (2015).
12. K. de L. Kristiansena, A. Woutersea, A. Philipse. Simulation of random packing of binary sphere mixtures by mechanical contraction. *Physica A* **358**, 249 (2005).
13. Z. Lingley, S. Lu, A. Madhukar. The dynamics of energy and charge transfer in lead sulfide quantum dot solids. *J. Appl. Phys.* **115**, 084302 (2014).
14. J.E. Lewis, S. Wu, X.J. Jiang. Unconventional gap state of trapped exciton in lead sulfide quantum dots. *Nanotechnology* **21**, 455402 (2010).
15. M. Abdellah, K.J. Karki, N. Lenngren *et al.* Ultra long-lived radiative trap states in CdSe quantum dots. *J. Phys. Chem. C* **118**, 21682 (2014).
16. Jian Zhang, Xiaomei Jiang. Confinement-dependent below-gap state in PbS quantum dot films probed by continuous-wave photoinduced absorption. *J. Phys. Chem. B* **112**, 9557 (2008).
17. N.V. Bondar, M.S. Brodyn, O.V. Tverdokhlibova, N.A. Matveevskaya, T.G. Beynik. Influence of a capping ligand on the band gap and excitonic levels in colloidal solutions and films of ZnSe quantum dots. *Ukr. J. Phys.* **64**, 425 (2019).
18. N.V. Bondar, M.S. Brodyn, N.A. Matveevskaya, T.G. Beynik. Efficient and sub-nanosecond resonance energy transfer in close-packed films of ZnSe quantum dots by steady-state and time-resolved spectroscopy. *Superlatt. Microstruct.* **130**, 106382 (2020).
19. S. Lu, A. Madhukar. Nonradiative resonant excitation transfer from nanocrystal quantum dots to adjacent quantum channels. *Nano Lett.* **7**, 3443 (2007).
20. J. Giblin, M. Kuno. Nanostructure absorption: A comparative study of nanowire and colloidal quantum dot absorption cross sections. *J. Phys. Chem. Lett.* **1**, 3340 (2010).
21. S.F. Wuister, C. de Mello Donega, A. Meijerink. Influence of thiol capping on the exciton luminescence and decay kinetics of CdTe and CdSe quantum dots. *J. Phys. Chem. B* **108**, 17393 (2004).
22. Y. Hinuma, A. Gruneis, G. Kresse, F. Oba. Band alignment of semiconductors from density-functional theory and many-body perturbation theory. *Phys. Rev. B* **90**, 155405 (2014).
23. Bo Li, P.J. Brosseau, D.P. Strandell, T.G. Mack, P. Kambhampati. Photophysical action spectra of emission from semiconductor nanocrystals reveal violations to the vavilov rule behavior from hot carrier effects. *J. Phys. Chem. C* **123**, 5092 (2019).
24. A.D. Dukes, M.A. Schreuder, J.A. Sammons *et al.* Pinned emission from ultrasmall cadmium selenide nanocrystals. *J. Chem. Phys.* **129**, 121102 (2008).
25. G.A. Beane, A.J. Morfa, A.M. Funston, P. Mulvaney. Defect-mediated energy transfer between ZnO nanocrystals and a conjugated dye. *J. Phys. Chem. C* **116**, 3305 (2012).
26. J.B. Hoffman, H. Choi, P.V. Kamat. Size-dependent energy transfer pathways in CdSe quantum dot-squaraine light-harvesting assemblies: Förster versus Dexter. *J. Phys. Chem. C* **118**, 18453 (2014).

Received 03.08.22.

Translated from Ukrainian by O.I. Voitenko

М.В. Бондар, М.С. Бродин,
Ю.П. Пирятинський, Н.А. Матвеевська

СТАЦІОНАРНА СПЕКТРОСКОПІЯ
ТА СУБНАНОСЕКУНДНИЙ РЕЗОНАНСНИЙ
ПЕРЕНОС ЕНЕРГІЇ ЕКСИТОННОГО
ЗБУДЖЕННЯ ВОДНИХ РОЗЧИНІВ
ТА ПЛІВОК НАНОКРИСТАЛІВ ZnSe

Тверді щільно-упаковані плівки напівпровідникових нанокристалів (НК) проявляють специфічні оптоелектронні властивості, зумовлені сильною квантовою взаємодією і гібридизацією орбіталей екситонів між НК. Це відкриває шляхи до створення нових штучних світлозбираючих комплексів та фотовольтаїчних структур з просторовим розділенням електронів та дірок. Метою даної роботи було дослідження колоїдних розчинів та твердих плівок НК ZnSe, стабілізованих тіогліцеролом, за допомогою стаціонарних та часороздільних вимірів оптичних спектрів. Ми виявили, що в розчинах НК переважає релаксація та рекомбінація екситонів через поверхневі та дефектні стани електронів та дірок, в той час як в плівках домінуючим каналом релаксації екситонів переважно є квантовий (внутрішній). Причина домінування останнього зумовлена швидким (субнаносекундним) переносом енергії екситонного збудження в плівках від менших НК до більших, що було встановлено через виміри спектрів фотолюмінесценції з розділенням у часі. Окрім цього, ми виявили два типи внутрішньоциліндричних станів екситонів у малих НК ZnSe, утворених окисленням та гідроксилюванням їхньої поверхні, і незвичайну “залежність” цих станів від розміру НК.

Ключові слова: енергія екситонного збудження, екситон, ZnSe, нанокристал.